HHS Public Access

Author manuscript

Mucosal Immunol. Author manuscript; available in PMC 2017 March 06.

Published in final edited form as:

Mucosal Immunol. 2017 March ; 10(2): 493–507. doi:10.1038/mi.2016.60.

TRPM2 Ion Channels Regulate Macrophage Polarization and Gastric Inflammation During Helicobacter pylori Infection

Susana Beceiro[1], **Jana N. Radin**[2], **Rupesh Chatuvedi**[2,#], **M. Blanca Piazuelo**[2], **Dennis J. Horvarth Jr.**[2], **Hanna Cortado**[1], **Yuanzheng Gu**[3], **Beverly Dixon**[2], **Chen Gu**[3], **Ingo Lange**[4], **Dana-Lynn T. Koomoa**[4], **Keith T. Wilson**[2,5,6], **Holly M. Scott Algood**[2,5,6,*,&], and **Santiago Partida-Sánchez**[1,7,*,&]

[1]Center for Microbial Pathogenesis, The Research Institute at Nationwide Children's Hospital, Columbus, OH

[2]Department of Medicine, Vanderbilt University School of Medicine, Nashville, TN

[3]Department of Neuroscience, College of Medicine, The Ohio State University, Columbus, OH

[4]The Daniel K. Inouye College of Pharmacy, University of Hawaii at Hilo, Hilo, HI

[5]Tennessee Valley Healthcare System, Department of Veterans Affairs, Nashville, TN

[6]Department of Pathology, Microbiology and Immunology, Vanderbilt University School of Medicine, Nashville, TN

[7]Department of Pediatrics, College of Medicine, The Ohio State University, Columbus, OH

Abstract

Calcium signaling in phagocytes is essential for cellular activation, migration and the potential resolution of infection or inflammation. The generation of reactive oxygen species (ROS) via activation of NADPH (nicotinamide adenine dinucleotide phosphate-) oxidase activity in macrophages has been linked to altered intracellular calcium concentrations. Because of its role as an oxidative stress sensor in phagocytes, we investigated the function of the cation channel transient receptor potential melastatin 2 (TRPM2) in macrophages during oxidative stress responses induced by *Helicobacter pylori* infection. We show that *Trpm2*$^{-/-}$ mice, when chronically infected with *H. pylori*, exhibit increased gastric inflammation and decreased bacterial

Correspondence: S Partida-Sanchez, Santiago.Partida-Sanchez@nationwidechildrens.org, or HMS Algood, holly.m.algood@vanderbilt.edu.

[#]Current Address: School of Biotechnology, Jawaharlal University, New Delhi, India

[&]These authors contributed equally to this work.

Disclosures

No conflicts of interest to declare. The contents in this study do not represent the views of the U.S. Department of Veterans Affairs or the United States Government.

Supplementary Material

Supplementary Information accompanies this paper.

Author contributions

S.B., H.M.S.A. and S.P-S. conceived and designed the project. S.B., J.N.R., R.C., M.B.P., D.J.H., H.C., Y.G., B.D. and I.L. Performed experiments. C.G., I.L., D-L.T.K. and K.T.W. Contributed in designing and supervising experiments. S.B., H.M.S.A. and S.P-S. Wrote the manuscript. All authors discussed and reviewed the manuscript.

colonization compared with WT mice. The absence of TRPM2 triggers greater macrophage production of inflammatory mediators and promotes classically activated macrophage M1 polarization in response to *H. pylori*. TRPM2-deficient macrophages upon *H. pylori* stimulation are unable to control intracellular calcium levels, which results in calcium overloading. Furthermore, increased intracellular calcium in TRPM2$^{-/-}$ macrophages enhanced MAPK and NADPH oxidase activities, compared to WT macrophages. Our data suggest that augmented production of ROS and inflammatory cytokines with TRPM2 deletion regulates oxidative stress in macrophages, and consequently, decreases *H. pylori* gastric colonization while increasing inflammation in the gastric mucosa.

Keywords

TRPM2 channel; Calcium homeostasis; oxidative-stress; macrophage; *Helicobacter pylori*

Introduction

The regulation of calcium (Ca^{2+}) influx across the plasma membrane is crucial for phagocyte activation and phagocyte-mediated immune responses. Cytosolic levels of Ca^{2+} control a diverse range of cellular processes, including chemotaxis, adhesion, phagocytosis, and the secretion of pro- and anti-inflammatory cytokines in phagocytic cells [1, 2]. In addition to the main channels responsible for Ca^{2+} entry, the store-operated CRAC (Ca^{2+} release-activated Ca^{2+}) channels [3], some members of the transient receptor potential (TRP) channel superfamily (TRPM2, TRPM4, TRPM7, TRPV2, TRPC1) are indispensable components in the regulation of Ca^{2+} homeostasis significantly impacting the function of macrophages [4, 5].

Transient receptor potential melastatin 2 (TRPM2) is a non-selective, Ca^{2+} permeable cation channel with an adenosine diphosphate ribose (ADPR) pyrophosphatase enzymatic NUDIX site at the C terminus domain [6, 7, 8]. TRPM2 is activated upon the direct binding of intracellular ADPR [6, 7] and indirectly under conditions of oxidative stress via the formation of H_2O_2, and thus, can function as an oxidative stress sensor [9, 10, 11]. TRPM2 is highly expressed in specialized phagocytic cells[8, 12, 13]. Phagocytes expressing TRPM2 respond to ROS secreted at inflammatory sites by releasing cytokines and chemokines, which play essential roles in the outcome and resolution of inflammation especially in mucosal tissues [8, 11, 14].

Detailed characterization of TRPM2-genetically deficient mice in different inflammatory models has revealed the involvement of this channel in various aspects of innate immunity. In the dextran sulfate sodium (DSS)-induced colitis model, *Trpm2*$^{-/-}$ mice were less susceptible to tissue ulceration [8]. In inflammatory and neuropathic pain models, *Trpm2*$^{-/-}$ mice displayed an impaired cellular infiltration [15]. In contrast, *Trpm2*$^{-/-}$ mice are more vulnerable to infection with *Listeria monocytogenes* than wild-type (WT) mice [16]. Di, *et al* proposed that TRPM2 protects mice in an endotoxin-induced lung inflammation model through inhibition of the membrane NAPDH-oxidase complex in phagocytic cells [11]. The diversity of these findings suggests that TRPM2 may play distinct roles under different

inflammatory situations. It is therefore important to clarify the mechanisms by which TRPM2 activation may exert a pro- or anti-inflammatory function in mucosal tissues.

Many bacterial infections stimulate NADPH oxidase activity in phagocytes to produce a burst of superoxide anions ($O_2^{\cdot-}$) that are converted into H_2O_2, which contributes to oxidative stress and the development of inflammation. *Helicobacter pylori* infection of the gastric mucosa triggers a vigorous innate and adaptive immune response characterized by local increase of oxidative stress, and the accumulation of PMNs, macrophages, and lymphocytes [17]. Both the immune response and the bacterium itself contribute to the elevated levels of ROS and reactive nitrogen species (RNS) within the infected gastric mucosa [18]. Moreover, excessive oxidative and nitrosative stress within the *H. pylori*-infected gastric mucosa correlate with mucosal damage and bacterial burden. The induction of inducible nitric oxide synthase (iNOS) and NADPH oxidase responses by *H. pylori* in the gastric mucosa provide an ideal milieu to test the ability of the oxidative stress-activated cation channel TRMP2 to regulate the immune response to *H. pylori*.

This study investigated how TRPM2-mediated functions affect the immune response and pathogenesis of chronic *H. pylori* infection in a mouse model. Our findings reveal that *H. pylori* activate TRPM2 in macrophages. However, the loss of TRPM2 results in increased *H. pylori*-induced gastritis and decreased bacterial colonization in mice. Importantly, chronically *H. pylori*-infected *Trpm2*$^{-/-}$ mice exhibit augmented inflammatory cytokine production, enhanced NADPH oxidase activity, and increased macrophage recruitment compared to *H. pylori*-infected WT mice. The absence of TRPM2 in macrophages results in enhanced production of ROS and activation of MAPKs in response to *H. pylori*. TRPM2$^{-/-}$ macrophages show increased baseline and *H. pylori*-induced intracellular Ca^{2+} levels compared to WT macrophages. Our findings suggest that TRPM2 mediates Ca^{2+} homeostasis and plasma membrane currents that are essential in regulating NADPH activity. Moreover, TRPM2 impacts the production of ROS and inflammatory cytokines, which subsequently mediate the gastric colonization and inflammatory damage of the gastric mucosa during *H. pylori* infection.

Results

TRPM2 deficiency favors inflammatory profile and M1 macrophage polarization

Macrophages polarize to classically activated (M1) macrophages by bacterial stimulation or to alternatively activated (M2) macrophages by parasite infection, tissue remodeling or tumor progression [19, 20]. To determine whether TRPM2$^{-/-}$ bone marrow-derived macrophages (BMDM) can polarize toward classical or alternative macrophage activation *in vitro*, BMDM from WT and *Trpm2*$^{-/-}$ mice were treated with M1- (LPS plus IFN-γ) or M2- (IL-4 plus IL-13) polarizing stimuli, and gene expression was assessed by quantitative real-time PCR (qRT-PCR). The combination of expression of the M1-associated markers, *Il6, Tnfa* and *Nos2*, was significantly enhanced in TRPM2$^{-/-}$ macrophages compared to WT macrophages (Figure 1a). Furthermore, the absence of TRPM2 led to a significant reduction of the M2-specific marker *Arg1* compared to WT macrophages (Figures 1a). Furthermore, the production of NOS protein was markedly increased in TRPM2$^{-/-}$ when compared to WT BMDM, under M1-stimulating conditions. TRPM2$^{-/-}$ macrophages produced slightly

increased NOS protein even under M2 stimulation (Figure 1b). In contrast, Arg1 protein production was greater in WT as compared to TRPM2$^{-/-}$ BMDM, under M2-stimulating conditions (Figure 1b). Together, these data suggest that TRPM2$^{-/-}$ macrophages are refractory to M2 polarization or predisposed to polarize to M1-like subset regardless of stimulation. To determine whether TRPM2$^{-/-}$ BMDM were prone to M1 polarization during differentiation in culture, we harvested unstimulated WT and TRPM2$^{-/-}$ macrophages after 7 days in culture, then measured the relative mRNA levels of the M1-associated markers, *Il1b, Il6, Tnfa* and *Nos2*. Neither M1 inflammatory cytokines nor *Nos2* were significantly elevated in unstimulated TRPM2$^{-/-}$ BMDM (Supplemental Figure S1). Since the roles of ROS-sensitive TRPM2 during chronic inflammation are controversial, we next evaluated macrophage function during co-culture with *H. pylori*, a bacterium that induces a strong oxidative response and activates gastric inflammatory response initiated by macrophages *in vivo* [21, 22]. To assess the effects of TRPM2 deficiency on the production of inflammatory mediators by macrophages, we measured the expression levels of pro-inflammatory cytokines in WT and TRPM2$^{-/-}$ BMDM co-cultured with *H. pylori,* and compared it to uninfected controls respectively. TRPM2$^{-/-}$ BMDM demonstrated a markedly enhanced expression of *Tnfa, Il6* and *Il12p40* in response to *H. pylori* (Figure 1c). Having observed *H. pylori* infected *Trpm2*$^{-/-}$ mice showed increased expression of pro-inflammatory macrophage markers, we hypothesized that TRPM2$^{-/-}$ macrophages may exhibit enhanced bactericidal activity. Thus, we performed bactericidal killing assays in WT and TRPM2$^{-/-}$ BMDM. After 4 h of co-culture with *H. pylori*, TRPM2$^{-/-}$ BMDM had a significant increase in bacterial killing compared to WT BMDM (Figure 1d).

Chronically infected *Trpm2*$^{-/-}$ mice exhibit increased gastritis and decreased *H. pylori* colonization

The role of TRPM2 in regulating the immune response has been highly divergent depending on the model of inflammation evaluated. To determine the direct impact of TRPM2 the chronic inflammatory process during *H. pylori*-induced gastric inflammation, WT and *Trpm2*$^{-/-}$ mice were orogastrically inoculated with *H. pylori* strain PMSS1. Histological examination of their stomach tissue at serial time points up to 6 months revealed that infection induced gastritis in both strains of mice, but *H. pylori*-infected *Trpm2*$^{-/-}$ mice had significantly more inflammation compared to *H. pylori*-infected WT mice at 1-month (mo) post infection (Figures 2a, b). To determine if these changes in inflammation influenced control of the infection, *H. pylori* colonization levels were measured. *Trpm2*$^{-/-}$ mice exhibited significantly lower bacterial burden compared to WT mice at all times post infection (Figure 2c). Notably, increased gastritis correlated significantly with decreased bacterial colonization in *Trpm2*$^{-/-}$ mice at 1-mo post infection, but there was no correlation in WT mice (Figure 2d). These data indicate that loss of TRPM2 results in more severe inflammation within the context of *H. pylori* infection and further suggests that the increased inflammation leads to reduced bacterial burden.

Loss of TRPM2 alters the gastric cytokine profile and iNOS production in *H. pylori*-infected mice

The increased gastritis in *H. pylori*-infected *Trpm2*$^{-/-}$ mice at 1-mo post infection, a time point when inflammatory recruitment is also driven by the adaptive response, also correlated

with significantly greater numbers of gastric F4/80$^+$ macrophages compared with infected WT mice, as assessed by flow cytometry (Figure 3a) and immunofluorescence (Supplemental Figure S2). TRPM2 was hypothesized to be an essential component in macrophage polarization during *H. pylori* infection *in vivo*. To test this, expression of gene markers associated with M1-like and M2-like polarization were assessed by qRT-PCR on positively selected F4/80$^+$ macrophages from *H. pylori*-infected mice at 1mo post infection (Figure 3b). Gastric macrophages isolated from *H. pylori*-infected *Trpm2*$^{-/-}$ mice expressed significantly higher levels of M1-associated genes; *Il1b* and *Nos2*, compared with macrophages isolated from *H. pylori*-infected WT mice (Figure 3b). Immunofluorescence analysis on the antrum of infected animals revealed greater accumulation of F4/80$^+$/iNOS$^+$ infiltrating macrophages in the tissue of *Trpm2*$^{-/-}$ mice than in the WT (Supplemental Figure S2a–b). In contrast, expression of *Arg1* was significantly decreased in TRPM2$^{-/-}$ macrophages compared to WT macrophages (Figure 3b).

To investigate how innate and adaptive immune responses were affected by the loss of TRPM2 leading to increased inflammation in the gastric mucosa among *H. pylori*-infected mice, levels of the pro-inflammatory cytokines were measured (Figure 3c). Expression of *Il6* was significantly increased in the stomachs of infected *Trpm2*$^{-/-}$ mice at the 1-mo time point. While quantification of *Il1b* revealed a trend toward increased expression of this cytokine in the *Trpm2*$^{-/-}$ mice at 3-mo after the infection, as compared to infected WT, such differences did not reach statistical significance (p=0.0597).

On the other hand, increased innate pro-inflammatory cytokines did not translate to increased Th1 or Th17 responses in the *Trpm2*−/− mice compared to WT mice. *Ifng* was significantly lower at 3-mo post infection in *H. pylori* infected *Trpm2*$^{-/-}$ mice compared to *H. pylori*-infected WT mice. *H. pylori* infection elicits a mixed of adaptive Th1, Th2, Treg and Th17 responses in the gastric mucosa [23]. Consistent with a previous report [24], levels of *Il17a* were increased in all *H. pylori*-infected mice, but there were no differences between the WT and *Trpm2*$^{-/-}$ mice. Interestingly, *Il10* and the transcriptional regulator of Treg cells, *Foxp3*, were expressed at significantly higher levels in *Trpm2*$^{-/-}$ mice compared to WT mice at 1 and 3-mo after infection. Taken together, these data suggest that the exacerbated inflammatory response observed in *H. pylori*-infected *Trpm2*$^{-/-}$ mice is likely a result of hyper-inflammatory innate immune cell activity rather than pro-inflammatory Th1 or Th17 cytokines. Moreover, increased activation of macrophages and ROS production may drive a stronger Treg response in the TRPM2−/− mice during *H. pylori* infection.

TRPM2 protects against excessive NADPH oxidase activity and ROS production in *H. pylori* infection

The TRPM2 channel's function in macrophages is linked to NADPH activity, ROS production, and subsequent cytokine and chemokine expression [7, 9, 10, 11]. Moreover, since ROS production is known to be involved in the development of gastric inflammation during *H. pylori* infection [25] we sought to define whether chronic *H. pylori* infection leads to changes in components of the oxidative burst pathway. Significantly greater levels of NADPH oxidase 2 (*Nox2*/gp91phox/CYBB) mRNA were detected in *H. pylori*-infected *Trpm2*$^{-/-}$ mice compared with *H. pylori* -infected WT mice at 3-mo post infection (Fig. 4a).

Likewise, when cultured with *H. pylori,* TRPM2$^{-/-}$ BMDM had significantly higher expression of *Nox2* mRNA compared to WT BMDM (Fig. 4b). To test the hypothesis that macrophages from *Trpm2*$^{-/-}$ mice might also exhibit increased ROS production in response to *H. pylori*, ROS production was measured in BMDM co-cultured with *H. pylori* using CellROX. We observed significantly increased ROS generation in TRPM2$^{-/-}$ macrophages co-cultured with *H. pylori* compared to WT macrophages (Fig. 4d). Similarly, *H. pylori*-infected or PMA-stimulated TRPM2$^{-/-}$ macrophages have significantly higher intracellular H_2O_2 levels (Figs. 4e–f). Conversely, pretreatment with diphenyleneiodonium (DPI), an NADPH oxidase inhibitor [26], abrogated the enhanced ROS production and *Nox2* expression in TRPM2$^{-/-}$ and WT macrophages co-cultures with *H. pylori* (Fig. 4c and 4d).

Since augmented ROS production has been correlated to increases in pro-inflammatory cytokine production [27, 28], we measured the gene expression of *Tnfa* in BMDM stimulated with *H. pylori* in the presence or absence of DPI treatment. Pretreatment with DPI diminished the expression of *H. pylori*-induced *Tnfa* in both TRPM2$^{-/-}$ and WT BMDM (Fig. 4g), indicating that the increase in *Tnfa* in the TRPM2$^{-/-}$ macrophages is dependent on ROS production. Moreover, in the presence of DPI, protein levels of iNOS were significantly reduced in M1 and M2-polarized TRPM2$^{-/-}$ BMDM and WT BMDM (Fig. 4h). These results suggest that TRPM2-dependent signaling may be important downregulating expression of pro-inflammatory mediators, and therefore, important for reducing gastric damage during *H. pylori*-infection through NADPH oxidase-mediated ROS downregulation.

TRPM2 negatively regulates *H. pylori* induced ERK, JNK and p38 activation

In addition to the abundant evidence for activation of elements of the MAPK system by NADPH oxidases [29, 30], *H. pylori* has been reported to activate the MAPK superfamily [31, 32, 33]. Thus, we hypothesized that exacerbated TRPM2$^{-/-}$ macrophage inflammatory responses may result in enhanced MAPK signaling in response to *H. pylori.* Indeed, co-cultured of BMDM with *H. pylori* increased ERK1/2, p38 and JNK activation in WT and TRPM2$^{-/-}$ BMDM (Figures 5a, 5c). Unlike WT BMDM, TRPM2$^{-/-}$ BMDM demonstrate constitutive ERK, p38 and JNK phosphorylation, which was enhanced and prolonged after co-culture with *H. pylori* compared to WT macrophages (Figures 5a, 5c). Quantitative densitometry demonstrated a marked increase in phosphorylation of MAPKs in TRPM2$^{-/-}$ BMDM compared with WT BMDM (Figures 5a–5c). DPI treatment decreased the phosphorylation level of ERK1/2 induced by *H. pylori* at selected time points in WT and TRPM2$^{-/-}$ BMDM (Figure 5d), suggesting that the altered MAPK signaling observed in TRPM2$^{-/-}$ BMDM is dependent on NADPH activity and ROS production.

H. pylori-activated TRPM2 channels are required for intracellular Ca^{2+}homeostasis in macrophages

To establish the functional link between TRPM2 and the Ca^{2+} responses orchestrated by *H. pylori* infection in macrophages, we first assessed the presence of the TRPM2 channel in response to *H. pylori* stimulation in these cells. As previously reported [10], we confirmed that the channel is constitutively expressed in mouse macrophages. Furthermore, we observed that only M2 polarization of macrophages increased TRPM2 transcripts levels compared to

M1 or *H. pylori*-infected macrophages (Supplemental Figure. S3a). This TRPM2 expression pattern was also observed in human M2 macrophages (Supplemental Figure. S3b), suggesting enhanced TRPM2 expression might favor anti-inflammatory phenotype in macrophages.

Because TRPM2 is involved in the modulation of Ca^{2+} homeostasis, we sought to determine the specific contribution of the channel by measuring the intracellular Ca^{2+} concentration ($[Ca^{2+}]_i$) in *H. pylori* stimulated WT and TRPM2$^{-/-}$ macrophages. *H. pylori* triggered a small, but detectable increase in $[Ca^{2+}]_i$, which rapidly declined to baseline levels in both WT and TRPM2$^{-/-}$ macrophages, as indicated by increased fluorescence of the Ca^{2+} indicator Fluo-3AM (Figure 6a). This Ca^{2+} signal represents release of Ca^{2+} from intracellular stores, since these experiments are performed in Ca^{2+}-free medium. Importantly, TRPM2$^{-/-}$ macrophages showed an increase in both baseline and *H. pylori*-stimulated responses, as indicated by the higher relative fluorescence. Addition of extracellular Ca^{2+} resulted in higher Ca^{2+} entry from the plasma membrane, which gradually declined over the next 4 min in *H. pylori*-stimulated WT BMDM (Figure 6b, blue trace). In contrast, in TRPM2$^{-/-}$ BMDM (red trace), Ca^{2+} entry was increased at a slower rate, and $[Ca^{2+}]_i$ remained elevated for at least 4 min after *H. pylori* stimulation. Similar results were observed when macrophages were maintained under Ca^{2+}-free conditions, and then spiked with $CaCl_2$ (2 mM) (Figure 6c) only, or with $CaCl_2$ (2 mM) followed by *H. pylori* (Figure 6d) at the indicated times.

These data suggest that lack of functional TRPM2 channels in macrophages leads to Ca^{2+} dysregulation and subsequent increases in $[Ca^{2+}]_i$ following *H. pylori* infection may be one of the mechanisms by which Ca^{2+}-dependent macrophage functions are being affected in TRPM2$^{-/-}$ macrophages.

To investigate the activity of the TRPM2 channel in the plasma membrane of macrophages upon *H. pylori* infection, we measured whole-cell currents in WT and TRPM2$^{-/-}$ macrophages using patch-clamp electrophysiology. First, current activation induced by intracellular perfusion of 200 μM ADPR, the specific agonist of TRPM2, showed a linear current-voltage relationships with a reversal potential and around 0 mV, which is characteristic for TRPM2 (Figure 7a) [6]. Because *H. pylori* stimulation induced intracellular Ca^{2+} release followed by robust plasma membrane Ca^{2+} entry as in Figure 6b, we reasoned that *H. pylori* might trigger extracellular Ca^{2+} uptake via TRPM2 and/or additional plasma membrane channels. To test the participation of TRPM2 in Ca^{2+} entry mediated by *H. pylori* stimulation, voltage-clamped macrophages derived from WT or *Trpm2*$^{-/-}$ mice were perfused with a solution containing *H. pylori*. Interestingly, the application of solution containing *H. pylori* evoked currents that were higher in amplitude compared to ADPR-induced WT macrophages but resembled the characteristic current –voltage relationship of TRPM2 [6] (Figures 7b, 7d). Stimulation of TRPM2$^{-/-}$ macrophages with *H. pylori* induced minimal development of whole-cell currents compared to WT macrophages (Figure 7b). The data suggest that TRPM2-mediated currents contribute significantly to *H. pylori*-induced current activation, and likely impact downstream regulation of Ca^{2+} dependent macrophage functions.

H_2O_2, which is known to increase intracellular ADP-ribose formation, can be generated through activation of the NADPH oxidase. To confirm whether *H. pylori* induced NADPH oxidase might subsequently result in opening of TRPM2 channels, we tested the effects of DPI on TRPM2 current development by whole-cell patch-clamp electrophysiology. When WT macrophages were perfused with *H. pylori*, TRPM2 currents developed to an average peak current of approximately 20pA/pF, over a range of time between 0–700s (Figure 7c). Interestingly, DPI pre-treated cells failed to develop TRPM2 currents after application of *H. pylori* (Figures 7c, d). The current-voltage (I-V) relationship was characteristic of TRPM2 channels (Figure 7d), and DPI-pretreated cells showed little to no inward or outward currents (Figure 7d), suggesting that NADPH oxidase activity and H_2O_2 production in response to *H. pylori* are required for the activation of TRPM2- dependent signaling.

To test the hypothesis that Ca^{2+} overloading observed in *H. pylori* stimulated TRPM2$^{-/-}$ macrophages is mediated through another ion channel at the plasma membrane; we investigated the expression and function of TRPM7 in BMDM. Previous studies have shown that TRPM7 plays a role in regulating ROS, nitric oxide production, and inflammation [34, 35, 36]. To examine TRPM7 regulation in TRPM2$^{-/-}$ and WT macrophages, we first evaluated TRPM7 protein expression in BMDM. Western blotting for TRPM7 protein expression on cell lysates indicated that TRPM7 expression was modestly upregulated in TRPM2$^{-/-}$ macrophages compared to WT (Supplemental Figure S4a). Nevertheless, electrophysiological patch-clamp measurements demonstrate that TRPM7 currents were significantly increased in TRPM2$^{-/-}$ macrophages (n=10) compared to WT macrophages (n=12). Peak TRPM7 currents were ~25pA/pF and ~12pA/pF in TRPM2$^{-/-}$ and WT macrophages, respectively (Supplemental Figure S4b). The current-voltage (I-V) relationship was characteristic of TRPM7, displaying an outwardly rectified current and very little inward current (Supplemental Figure S4c). These results suggest TRPM7 channel activity is increased in the absence of TRPM2, and may contribute to the Ca^{2+} overloading in these cells. In conclusion, our hypothetical working model (Figure 8) indicates that *H. pylori* stimulation induces strong NADPH oxidase function, and consequently TRPM2 activation, which in turn limits NADPH oxidase activity and prevents excessive inflammation (Figure 8a). In contrast, Ca^{2+} overloading in the TRPM2 deficient macrophages favors polarization toward the pro-inflammatory M1 phenotype, and concomitantly, this activity enhances oxidative stress through unregulated NADPH oxidase activity, followed by increased generation of intracellular ROS. Together, our data support the hypothesis that TRPM2 channels work as a functional cellular rheostat that controls ion currents at the plasma membrane, thereby regulating Ca^{2+} homeostasis and macrophage oxidative functions during *H. pylori* infection.

Discussion

Regulation of intracellular Ca^{2+} concentration is a tightly controlled process. However, the molecular players involved in shaping intracellular Ca^{2+} signals are poorly characterized in phagocytes. The current paradigm states that increases in cytosolic Ca^{2+} levels are caused by activation of cell surface receptor by endogenous or exogenous stimuli, which trigger the release of Ca^{2+} from endoplasmic reticulum (ER) Ca^{2+} stores, and is followed by Ca^{2+} entry through the plasma membrane via Ca^{2+} release-activated Ca^{2+} current (CRAC)

channels [37, 38, 39]. However, macrophages express a variety of additional ion channels including the transient receptor potential (TRP) channels, which have recently emerged as essential regulators of important physiological functions in macrophages [4, 5]. In addition to conducting ions through the plasma membrane, some TRP channels may also function to couple ER-to-plasma membrane signaling crosstalk or to release Ca^{2+} from internal stores contributing to global cellular Ca^{2+} homeostasis [5, 40]. Specific members of the TRPM and TRPC subfamilies have been associated with Ca^{2+} mobilization functions in phagocytic cells including, chemotaxis, phagocytosis, and cytokine secretion [41, 42].

We previously reported that TRPM2, a nonselective Ca^{2+}-permeable channel abundantly expressed in phagocytic cells, plays essential roles in chemotaxis of PMNs, macrophages and DCs [14, 43], and during activation and maturation of dendritic cells [14]. Because TRPM2 has been extensively proposed as an oxidative stress sensor and *H. pylori* infection causes oxidative stress in the gastric mucosa, we addressed the function of TRPM2 in macrophages using *H. pylori* infection as our chronic inflammation model. Our findings show that the loss of TRPM2 results increased *H. pylori*-induced gastritis and decreased bacterial colonization in mice. Indeed, gastritis inversely correlated with bacterial colonization density in the *Trpm2*$^{-/-}$ mice. These data also support the finding that TRPM2$^{-/-}$ macrophages demonstrated increased bacterial killing activity, augmented levels of pro-inflammatory cytokines compared to WT macrophages, indicating TRPM2 has a regulatory and anti-inflammatory function.

Although other research groups had previously attempted to elucidate the effects of TRPM2 in distinct models of inflammation or infection [8, 11, 44, 45], these studies have yield conflicting results. Yamamoto and colleagues reported the first TRPM2 deficient mouse model [8]. The initial studies showed that ROS-dependent activation of TRPM2 was crucial for chemokine production in mouse monocytes. Moreover, ROS-induced Ca^{2+} influx through TRPM2 triggered Ca^{2+}- dependent tyrosine kinase Pyk2 and Erk signaling, and thus led to the inflammatory nuclear translocation NF-κB. Monocytes of *Trpm2*$^{-/-}$ mice also displayed a reduced production of the chemokine CXCL2, homolog to human CXCL8. Interestingly, *Trpm2*$^{-/-}$ mice upon DSS–induced colitis exhibited reduced release of IFN-γ and IL-12 cytokines. In addition, in this DSS model, neutrophil infiltration, and ulceration were attenuated in *Trpm2*$^{-/-}$ mice compared to WT mice, suggesting that TRPM2 may aggravate inflammation. Another study supporting a pro- inflammatory role for TRPM2 demonstrated that TRPM2 function and Ca^{2+} entry were also required for LPS-induced production of IL-6, TNF-α, IL-8, and IL-10 in human monocytes [46]. These data shed little light on the mechanism by which TRPM2 positively regulates secretion of inflammatory cytokines in response to DSS or LPS. In both cases, however, increased intracellular levels of Ca^{2+} appeared to play a critical role in activating such cytokine secretion. More recently, another TRPM2 deficient mouse was generated by GlaxoSmithKline (GSK). The first report using these animals showed that the absence of TRPM2 exacerbated inflammation in the lungs of mice systemically exposed to LPS. In addition, authors also found increased amounts of the pro-inflammatory cytokines CXCL2, TNF-α, and IL-6 in the lungs of *Trpm2*$^{-/-}$ mice [11]. Furthermore, NADPH oxidase mediated production of ROS was greater in the lungs and BMDM isolated from *Trpm2*$^{-/-}$ as compared to WT mice. They proposed TRPM2 inhibits ROS production in macrophages through TRPM2 induced plasma

membrane depolarization dampening NADPH-oxidase activity [11]. While the chronic elevation of ROS in the *H. pylori* model presented here could contribute to gastritis and tissue damage it may also explain the increased level of Tregs and therefore, the reduction in Th1 responses. It has been demonstrated that Tregs are hyper functional in elevated levels of ROS [47, 48], and therefore, oxidative stress may actually trigger Tregs, which are poised to suppress the excessive inflammation in the TRPM2 KO mice.

While LPS is widely accepted as a model of endotoxin-mediated inflammation, differences in routes of LPS administration, doses, experimental readouts, limit the reproducibility of the model and do not mimic the natural response to an infection. Therefore, we turned to a chronic persistent bacterial infection model to investigate how TRPM2 affects inflammation and oxidative stress responses. Our data demonstrate that TRPM2$^{-/-}$ macrophages exhibit strong functional M1 polarization characterized by increased production of iNOS and enhanced NADPH oxidase activity via upregulation of NOX2, which resulted in greater accumulation of ROS. Positive regulation of NADPH oxidase correlated with an early and prolonged phosphorylation of MAPK ERK, p38, and JNK in response to *H. pylori* in TRPM2$^{-/-}$ as compared to WT macrophage responses. Despite the fact that we have used *Trpm2*$^{-/-}$ mice reported by Yamamoto *et al.* [8] in our studies, data is in good agreement with findings on *Trpm2*$^{-/-}$ mice from GSK, wherein TRPM2 activation down regulates macrophage inflammatory functions by restricting NADPH oxidase function. However, Perraud and colleagues by using GSK animals reported increased morbidity and mortality in *Trpm2*$^{-/-}$ mice upon *i.v.* injection of *L. monocytogenes* [44]. Although suppressed production of IFN-γ, IL-12 and iNOS were correlated with increased bacterial burden and greater *Trpm2*$^{-/-}$ mice mortality, septicemia was not evaluated as possible cause of death in *L. monocytogenes* infected *Trpm2*$^{-/-}$ mice [44]. Clearly the origin of the *Trpm2*$^{-/-}$ mouse models available may not be the only condition to consider for the experimental discrepancies observed.

Previously published data suggest that TRPM2 facilitates plasma membrane depolarization [11] and this poses a potential explanation of how TRPM2 deficiency leads to increased NADPH oxidase and enhanced ROS production in our model. An additional mechanism, which can further explain enhanced oxidative responses in the absence of TRPM2, is the disruption of Ca^{2+} homeostasis in phagocytes. Indeed, increases in $[Ca^{2+}]_i$ levels and the activation of Ca^{2+} - dependent PKC and its downstream MAPK have been directly associated to induction of NADPH oxidase activity [49]. We surmised that TRPM2-mediated membrane depolarization is a transient event that may not fully account for the chronic inflammatory state of the macrophages or, the strong M1 polarization and resistance to M2 conversion observed in TRPM2$^{-/-}$ macrophages. Since uptake of Na^+ via TRPM2 results in membrane depolarization, and thereby reduces Ca^{2+}entry, we reasoned that TRPM2$^{-/-}$ cells lacking this regulatory pathway upon stimulation may undergo transitory Ca^{2+} starvation, therefore be prone to Ca^{2+} overloading, and consequently, altered Ca^{2+} homeostasis (hypothetical model depicted in Figure 8). As predicted, at baseline, TRPM2$^{-/-}$ macrophages exhibited slightly increased intracellular Ca^{2+} levels, ROS production, and MAPK phosphorylation. Strikingly, addition of *H. pylori* induced a moderate transient spike of Ca^{2+} release followed by large and prolonged influx of Ca^{2+} resulting in a significant increase in intracellular Ca^{2+} levels in the TRPM2$^{-/-}$ macrophages, whereas Ca^{2+} influx in

the WT cells returned to baseline levels after few minutes. Together, these data suggest that TRPM2 mediates membrane currents and Ca^{2+} homeostasis in macrophages and thereby regulates NADPH activity. Similar to TRPM2, another member of the TRPM subfamily, TRPM4, was reported to perform Ca^{2+} regulatory function in DCs [50]. Notably, bacterial stimulation, but not LPS, induced Ca^{2+} overloading in $TRPM4^{-/-}$ DCs [50]. Likewise, we observed changes in intracellular Ca^{2+} levels and TRPM2 developed currents by electrophysiological patch clamp measurements when the cells were stimulated with *H. pylori.* These data highlight the idea that bacterial, as opposed to endotoxin-induced, stimulation of macrophages recapitulates better the signaling pathway during natural infection and inflammation.

The molecular mechanism mediating extracellular Ca^{2+} entry activates NADPH oxidase activity is not completely understood; however, several published studies have provided evidence for the requirement of extracellular Ca^{2+} entry for NADPH oxidase activation [51, 52, 53]. The link between Ca^{2+} entry and NADPH oxidase activation is further supported by a significant decrease of superoxide anion production when extracellular Ca^{2+} is suppressed or chelated by EGTA [53]. Additional plasma membrane channels that conduct the required Ca^{2+} signal enhancing NADPH oxidase, may contribute to Ca^{2+} overloading in $TRPM2^{-/-}$ macrophages. An additional member of the TRPM subfamily TRPM7 is expressed at the plasma membrane in macrophages and has been linked to oxidative stress responses [54]. TRPM7 is a Ca^{2+} and Mg^{2+} permeable ion channel modulated by $PI(4,5)P_2$ during cellular activation. Interestingly, TRPM7 currents are markedly enhanced by H_2O_2 exposure [54]. In fact, the mRNA and protein expression of TRPM7 are increased in cells exposed to oxidant agents, whereas decreasing TRPM7 levels has been reported to yield a concomitant decrement in intracellular ROS levels [55], suggesting a positive feedback for TRPM7 activity in an oxidant environment. Thus, the Ca^{2+} overload, increased ROS production, and phosphorylation of ERK and JNK observed in macrophages from *Trpm2*$^{-/-}$ mice may be mediated by increased TRPM7 activity.

In summary, it is clear that regulation of the oxidative stress response by phagocytes is vital for controlling tissue damage in chronic bacterial infections. Here using *H. pylori* as infection model, we provide novel insight into oxidative stress regulation by phagocytes via the oxidant-activated nonselective cation channel TRPM2. The absence of TRPM2 results in altered calcium homeostasis, and enhanced macrophage production of ROS and inflammatory cytokines associated with increased gastric inflammation in *H. pylori*-infected *Trpm2*$^{-/-}$ mice. The absence of TRPM2 in macrophages stimulates production of inflammatory mediators and promotes classically activated macrophage M1 polarization in response to *H. pylori*. Increased intracellular Ca^{2+} levels in $TRPM2^{-/-}$ macrophages upon *H. pylori* stimulation results in Ca^{2+} overloading, consistent with exacerbated macrophage's inflammatory response. Our data suggest that positive modulation of TRPM2 function may provide a therapeutic strategy to control excessive NADPH oxidase activity and reduce tissue damage. Alternatively, inhibition of TRPM2 could enhance oxidant mediated macrophage antimicrobial function during infection.

Methods

Mice

Mice deficient in TRPM2, C57BL/6J.129 *Trpm2*$^{-/-}$, were generated as described previously [8]. These mice were backcrossed greater than 9 generations at the time of these experiments. WT mice were backcrossed littermate controls housed in the same facilities throughout the experiments. Animals were maintained in the barrier facility at Nationwide Children's Hospital and the Vanderbilt University. Fecal samples were confirmed negative for intestinal Helicobacter by PCR (RADIL; University of Missouri). Feces from sentinel mice housed in the same room were routinely tested by PCR for pinworms, mouse parvovirus and several other murine pathogens, and consistently tested negative for each of these infections. For all the experiments, 6- to 8-week-old mice were used. The Institutional Animal Care and Use Committees of the Vanderbilt University and the Department of Veteran's Affairs IACUC (V/13/240), and the Research Institute at Nationwide Children's Hospital IACUC (00505AR) approved the animal study protocols.

Culture of *H. pylori*

H. pylori strain PMSS1 was used in all experiments[76]. Bacteria were grown on trypticase soy agar (TSA) plates containing 5% sheep blood. Alternatively, bacteria were grown in Brucella broth containing 5% heat-inactivated FBS and 10 μg/ml vancomycin. Cultures were grown at 37°C in either room air supplemented with 5% CO_2, or under microaerobic conditions generated by a GasPak EZ satchel (BD 260680).

H. pylori infection and tissue harvest

Helicobacter-free *Trpm2*$^{-/-}$ and WT mice, 8–10 w old, were used in all *in vivo* experiments. One day prior to infection of mice, *H. pylori* was inoculated into liquid medium and were cultured for 18 h under microaerobic conditions, as described above. Mice were orogastrically inoculated with a suspension of 5×10^8 CFU *H. pylori* (in 0.5 ml of Brucella broth) twice over 5 days. For 48 h time points, mice received one dose of PMSS1. At animal sacrifice, tissues were collected for various analyses including flow cytometry, cytokine expression analysis, histology (inflammation scoring), and isolation of gastric macrophages.

Processing of mouse stomach tissue

The stomach was removed from each mouse by excising between the esophagus and the duodenum. The forestomach was discarded. The glandular stomach was opened, rinsed gently in cold PBS, and cut into three longitudinal strips that were used for bacterial culture, RNA analysis, and histology. For culturing of *H. pylori* from the stomach, gastric tissue was placed into Brucella broth-10% FBS for immediate processing. Gastric tissue was stored in RNALater solution for subsequent RNA isolation.

Histology and immunofluorescence

A longitudinal strip from the greater curvature of the stomach was excised and placed in 10% normal buffered formalin for 24 h, embedded in paraffin and processed routinely for hematoxylin and eosin (H&E) or immunofluorescence staining. Double-labeled

immunofluorescence was carried out to localize F4/80 and iNOS expression in murine stomach. Samples were fixed with 2% paraformaldehyde for 15 min at room temperature. Samples were Tissue slides were then incubated overnight at 4°C with a biotin anti-mouse F4/80 antibody (1:150, Abcam) and a polyclonal rabbit anti-mouse iNOS antibody (1:200, Santa Cruz). Alexa Fluor 568 anti-mouse IgG and Streptavidin- FITC conjugate were used as secondary antibodies. Samples were mounted using Prolong Gold antifade reagent (Invitrogen). Samples were analyzed using the Zeiss 510 LSM Meta confocal laser scanning microscope and Zeiss LSM Image Browser program (Carl Zeiss, Hudson, OH, USA).

Indices of inflammation and injury were scored by a single pathologist (MP) who was blinded to the identity of the mice. Acute and chronic inflammation in the gastric antrum and corpus were graded on a 0–3 scale. Acute inflammation was graded based on density of neutrophils and chronic inflammation was graded based on the density of lamina propria mononuclear cell infiltration independent of lymphoid follicles. The total inflammation score is the sum of the chronic and acute inflammation scores in the antrum and the corpus.

Gastric macrophage isolation

For gastric macrophage isolations, the stomach removed from each mouse as described above. To dissociate the gastric tissue, the glandular stomach was cut with scissors into 2-mm pieces and digested for 20 min with 1 mg/ml dispase, 0.25 mg/ml collagenase A, and 25 U/ml DNase (Roche Diagnostics, Indianapolis, IN) at 37°C. The suspension was passed through a 70-μm cell strainer (BD Biosciences, San Diego, CA). Cells were harvested by centrifugation and washed with PBS containing 4% FBS. $F4/80^+$ cells were isolated using the MACs technology (Miltenyi Biotech). In brief, cells were labeled with biotin-conjugated anti-mouse F4/80 antibody (CALTAG Laboratories, Burlingame, CA). Cells were washed and incubated with streptavidin-conjugated magnetic beads. Cells were brought to a volume of 1 ml with cold MACs buffer, and cell suspensions were applied to an MACS column according to the manufacturer's instructions. The positive fraction was resuspended in DMEM cell culture medium without L-Arg, phenol red, or serum. In some experiments, the positive fraction was incubated with fluorescein isothiocyanate-conjugated monoclonal antibody to the leukocyte marker CD11b and allophycocyanin-conjugated monoclonal antibody to Gr-1, a marker for granulocytes. Cells were analyzed by flow cytometry to determine the percentage of positive cells using a BD LSRII system (BD Biosciences). Less than 2% were neutrophils. This procedure consistently lead to close to 90% macrophages (87–92%) as previously reported [56]. Total RNA was isolated using a VERSAGENE 96-well RNA purification kit (Gentra Systems, Minneapolis, MN) according to the manufacturer's instructions. cDNA was synthesized from RNA with an iScript cDNA synthesis kit (Bio-Rad). Three microliters of cDNA was used for a qRT-PCR for *iNOS, Arg1, Arg2, Il1b, YM-1* and *Gapdh*.

Flow cytometric analysis of gastric cellular infiltrates

Whole mouse stomachs were harvested and processed using Miltenyi's Gentle Dissociator (Miltenyi Biotec, Boston, MA). In brief, the stomach was cut into 5 mm pieces and then transferred to a C-tube (Miltenyi Biotec) in 5 ml RPMI/10% FBS. The preset Miltenyi Biotec program m_imptumor 02 was run once and then the tissue was digested for 30 min at

37°C in a solution containing (0.32 mg/ml Dispase and 0.30 mg/ml Collagenase D, Roche) while shaking in a CO2 incubator. After the 37°C incubation, 100U/ml of DNase (Sigma) was added to each tube and the Miltenyi Gentle Dissociator was run for a second and third time using the preset program m_imptumor 02. The tissue homogenate was passed through a 70 μm cell strainer (BD). Cells were harvested by centrifugation, washed, and then live cells were counted by using a hemocytometer and trypan blue exclusion staining. The samples were stained with 2 μg/ml anti- F4/80, 1.5 μg/ml anti-Gr1 (clone RB6-8C5), and 2 μg/ml anti-CD11b (clone M1/70) (all antibodies were purchased from BD Biosciences, and analyzed on a BD LSR II flow cytometer).

RNA extraction and qRT-PCR

RNA was isolated from the stomach and BMDM using the TRIZOL isolation protocol combined with the Qiagen RNA easy clean-up protocol. RNA was reverse transcribed using the High Capacity cDNA Reverse Transcription Kit (Applied Biosystems, Foster City, CA). For qRT-PCR, we used the relative gene expression method (Relative Units = $2^{-\Delta\Delta Ct}$). GAPDH served as the normalizer. All qRT-PCR was performed using an Applied Biosystems StepOne Plus instrument. Levels of cytokine expression are indicated as relative mRNA levels, based on comparison of tissue or cells from *H. pylori*-infected mice with tissue or cells from uninfected mice (calibrator tissue). Primer and probe sets were purchased as Taqman Gene Expression Assays from Applied Biosystems. Specific primers' GenBank accession number and assay ID are provided in Supplementary Table 1. For TRPM2, PCR reactions were performed using the specific primer pair mTRPM2 3380 sense 5′ – CAGATCCCAACCTACATTGACG- 3′ and mTRPM2 3594 antisense 5′-GAAGGTGTAGTTGAACATGGCGA-3′. A 215-bp TRPM2-PCR product was detected after 30 cycles of amplification: 30 s at 94°C, annealing for 30 s at 46°C, and extension for 40 s at 72°C, followed by a final extension for 10 min. For GADPH, PCR reactions used the specific primer pair mGADPH 563 sense 5′-ACCACAGTCCATGCCATCAC-3′ and mGADPH 1014 antisense 5′-TCCACCACCCTGTTGCTGTA-3′. A 451-bp GADPH-PCR product was detected after 30 cycles of amplification: 30 s at 94°C, annealing for 30 s at 53°C, and extension for 40 s at 72°C, followed by a final extension for 10 min.

Culture of *H. pylori* from mouse stomach

Gastric tissue was homogenized using a tissue tearor Biospec (BioSpec Products, Inc. Bartlesville, OK). Serial dilutions of the homogenate were plated on trypticase soy agar plates containing 5% sheep blood, 10 μg/ml nalidixic acid, 100 μg/ml vancomycin, 2 μg/ml amphotericin, and 200 μg/ml bacitracin. After 5 to 7 days of culture under microaerobic conditions, *H. pylori* colonies were counted.

Preparation and stimulation of BMDM

BMDM were generated from femurs and tibias of *Trpm2*$^{-/-}$ and WT mice. BM cells were cultured in RPMI1640 supplemented with 10% FBS, 100 U/ml penicillin, 100 μg/ml streptomycin, 2 mM L-glutamine, with the addition of 20% L929-cell–conditioned medium. After 5–7 days of culture, cells were seeded into 6-well tissue culture treated plates at a density of 2×10^6 cells/well in antibiotic-free medium overnight prior to infection. Macrophages were infected with live *H. pylori* strain PMSS1 at a multiplicity of infection

(MOI) of 10 to 100 bacteria/macrophage, as indicated. When indicated, macrophages were stimulated with 100 ng/ml LPS and 20 ng/ml IFN-γ, or 20 ng/ml IL-4 and 20 ng/ml IL-13. After incubation for the indicated time points, culture supernatants and cells pellets were collected and assayed as indicated.

Bactericidal assay

Infected BMDM with *H. pylori* at an MOI of 10 for 1 h at 37°C., were washed twice with PBS, and incubated for 0.5, 1, 2, and 4 hours in fresh medium containing gentamicin (100 μg/ml) to limit the growth of extracellular bacteria. After washing, macrophages were lysed in 1% Triton X100/PBS for 2 min at room temperature, and centrifuged at 1000 x g for 10 min at 4°C Bacteria were pelleted from the resulting supernatant by centrifugation at 10,000 x g for 10 min., resuspended in 20 μl of TBS and kept on ice. Bacteria viability was determined with the LIVE/DEAD BacLight Bacterial Viability kit (Molecular Probes), according to the manufacturer specifications, and samples were promptly read on a BD Biosciences LSR II flow cytometer. Data for side scattering, forward scattering, and fluorescence were acquired and analyzed with FlowJo software (Tree Star, Inc.).

Measurement of ROS production

BMDM were plated in non-tissue-culture-treated 12-well dishes and stimulated with *H. pylori* at different MOI for 4 h. Culture medium was removed, cells were washed with PBS, and then incubated with CellROX Green reagent (Invitrogen) at 5 μM final concentration in complete RPMI 1640 medium (Invitrogen) for 30 min at 37°C. For DPI assay, cells were incubated in the presence of 10 μM DPI for 1 h before and during the incubation with *H. pylori*. Cells were washed with warmed PBS (37°C), removed from plates with cold PBS containing 1 mM EDTA by pipetting, pelleted at 1,500 rpm for 3 min, immediately resuspended in cold PBS containing 1% FBS and subjected to flow cytometry analysis. Unstained controls were treated similarly, except that treatments and dyes were omitted. To control for baseline dye fluorescence, samples from each experiment were left unstimulated but stained according to the above procedure. As alternative method for ROS detection, BMDM were loaded for 30 min at 37°C with dihydro-rhodamine 123 (DHR123, Invitrogen) and stimulated for 30 min at 37°C with *H. pylori* at different MOI, 1 μM PMA, or 100μM hydrogen peroxide, as indicated. The production of ROS was quantified via flow cytometry by measurement of intracellular rhodamine. Flow cytometry data were acquired on a BD LSR II and analyzed using FlowJo software. Results are presented as mean channel fluorescence was normalized to the untreated WT. Error bars were generated by calculating SD of the mean from triplicate samples.

Western blot analysis

BMDM were stimulated with LPS plus IFN-γ, IL-4 plus IL-13, or *H. pylori* (MOI of 10), as indicated. When indicated, cells were pretreated with DPI (10 μM). Cells were washed twice with cold PBS, and then lysed in ice-cold modified RIPA buffer (50 mM Tris-HCl, pH 7.4, 1% Nonidet P-40, 0.5% sodium deoxycholate, 150 mM $NaCl_2$) containing protease inhibitors and phosphatase inhibitor cocktail set (Sigma). Proteins were separated by SDS-PAGE and transferred to nitrocellulose membranes. The membranes were incubated with primary antibodies at 4°C overnight, then washed with TRI-buffered saline, including 0.1%

Tween-20, exposed to peroxidase-conjugated secondary antibodies for 1 h at room temperature, washed, and then visualized using an Enhanced Chemiluminescence Plus kit (Thermo Scientific). Expression of iNOS, Arg1, and β-actin was determined using iNOS-specific antibody and Arg1-specific antibody. Activation of Erk, p38, and JNK was determined using phospho-Erk1/2-specific antibody, p38-specific antibody, and phospho-JNK-specific antibody. The total amount of Erk2 and p38 was detected by using Erk2-specific antibody and p38-specific antibody, respectively. Description of the antibodies used for Western blot is provided in Supplementary Table 2.

Intracellular Ca^{2+} measurement by flow cytometry

BMDM were resuspended in cell-loading media (HBSS with Ca^{2+} and $MgCl_2$ + 1% FBS + 4 mM probenecid) at 1×10^7 cells per ml. The cells were incubated at 37 °C for 30 min with Fluo-3AM (4 μg/ml) (Molecular Probes, Eugene, Oregon), washed twice and resuspended in cell- loading Ca^{2+}-free medium at 1×10^6 cells per ml. Cells were stimulated with *H. pylori* (MOI of 100), $CaCl_2$ (2mM), $MgCl_2$ (1.5mM), or ionomycin (1 μM) (Sigma). The accumulation of intracellular Ca^{2+} in individual cells was assessed by flow cytometry measuring the fluorescence emission of Fluo-3AM in the over 200 s. Data were analyzed using FlowJo's kinetic platform.

Electrophysiological recordings

Whole-cell patch-clamp recording was performed on BMDM obtained from WT and *Trpm2*$^{-/-}$ mice, using the same internal solution, Hank's buffer, recording protocols and the setup as previously described [57]. In voltage-clamp recording, the cells were initially held at −80 mV, given 200-ms voltage episodes in 10-mV increment from −100 mV to +100 mV, and then the I-V relationship was obtained. The capacitance and membrane potentials under the current-clamp mode were also measured.

For *H. pylori* induced TRPM2 currents in wild type macrophages (Figs 6C & 6D) the extracellular solution contained (in mM) 140 NaCl, 2.8 KCl, 1 $CaCl_2$, 1 $MgCl_2$, 10 HEPES-NaOH and 11glucose. For the intracellular solution (in mM) 130 Cs-Glutamate, 8 NaCl, 10 HEPES-CsOH and 1 $MgCl_2$ were used. Patch-clamp experiments were performed under whole- cell configuration at 21–25 °C using a HEKA EPC10 amplifier. Voltage ramps of 100 ms duration spanning from −100 to +100 mV were delivered at a rate of 0.5 Hz from a holding potential of 0 mV. Currents were normalized to cell size in pF. Data points for inward and outward current amplitudes were obtained at −80 and +80 mV respectively. Currents were normalized to the current obtained before development of current activation.

Statistical analysis

Four to thirteen mice per group per time point were used for all of the studies. To compare results obtained with different groups of mice, statistical analysis was performed using ANOVA followed by a student-unpaired *t*-test. For analyses of bacterial numbers, the data were normalized by log transformation prior to statistical analysis. For histology scores, the Mann-Whitney U-test was applied to compare results between *Trpm2*$^{-/-}$ mice and WT mice. Statistical analyses were performed using GraphPad Prism Software.

Supplementary Material

Refer to Web version on PubMed Central for supplementary material.

Acknowledgments

We thank Nationwide Children's Hospital and Vanderbilt University's Flow Cytometry and Histology Core Facilities. This work was supported by The National Institutes of Health, NIAID R01-AI092117 to S.P-S. and by Merit Review Grants from the Office of Medical Research, Department of Veterans Affairs. IBX000915A to H.M.S.A. and I01BX001453 to K.T.W. RC is supported by NIAID 1K01AT007324-01, D-L.K. is supported by K01CA154758-01A1 and K.T.W. is also supported by NIDDKD R01DK053620.

References

1. Freedman BD. Mechanisms of calcium signaling and function in lymphocytes. Crit Rev Immunol. 2006; 26:97–111. [PubMed: 16700648]
2. Feske S. Calcium signalling in lymphocyte activation and disease. Nat Rev Immunol. 2007; 7:690–702. [PubMed: 17703229]
3. Randriamampita C, Bismuth G, Trautmann A. Ca(2+)-induced Ca2+ release amplifies the Ca2+ response elicited by inositol trisphosphate in macrophages. Cell Regul. 1991; 2:513–522. [PubMed: 1782213]
4. Desai BN, Leitinger N. Purinergic and calcium signaling in macrophage function and plasticity. Front Immunol. 2014; 5:580. [PubMed: 25505897]
5. Feske S, Wulff H, Skolnik EY. Ion channels in innate and adaptive immunity. Annu Rev Immunol. 2015; 33:291–353. [PubMed: 25861976]
6. Perraud AL, et al. ADP-ribose gating of the calcium-permeable LTRPC2 channel revealed by Nudix motif homology. Nature. 2001; 411:595–599. [PubMed: 11385575]
7. Sano Y, et al. Immunocyte Ca2+ influx system mediated by LTRPC2. Science. 2001; 293:1327–1330. [PubMed: 11509734]
8. Yamamoto S, et al. TRPM2-mediated Ca2+influx induces chemokine production in monocytes that aggravates inflammatory neutrophil infiltration. Nat Med. 2008; 14:738–747. [PubMed: 18542050]
9. Sumoza-Toledo A, Fleig A, Penner R. TRPM2 channels are not required for acute airway inflammation in OVA-induced severe allergic asthma in mice. J Inflamm (Lond). 2013; 10:19. [PubMed: 23631390]
10. Kashio M, et al. Redox signal-mediated sensitization of transient receptor potential melastatin 2 (TRPM2) to temperature affects macrophage functions. Proc Natl Acad Sci U S A. 2012; 109:6745–6750. [PubMed: 22493272]
11. Di A, et al. The redox-sensitive cation channel TRPM2 modulates phagocyte ROS production and inflammation. Nat Immunol. 2012; 13:29–34.
12. Heiner I, et al. Expression profile of the transient receptor potential (TRP) family in neutrophil granulocytes: evidence for currents through long TRP channel 2 induced by ADP-ribose and NAD. Biochem J. 2003; 371:1045–1053. [PubMed: 12564954]
13. Massullo P, Sumoza-Toledo A, Bhagat H, Partida-Sanchez S. TRPM channels, calcium and redox sensors during innate immune responses. Semin Cell Dev Biol. 2006; 17:654–666. [PubMed: 17178241]
14. Sumoza-Toledo A, et al. Dendritic cell maturation and chemotaxis is regulated by TRPM2-mediated lysosomal Ca2+ release. FASEB J. 2011; 25:3529–3542. [PubMed: 21753080]
15. Haraguchi K, et al. TRPM2 contributes to inflammatory and neuropathic pain through the aggravation of pronociceptive inflammatory responses in mice. J Neurosci. 2012; 32:3931–3941. [PubMed: 22423113]
16. Knowles H, et al. Transient Receptor Potential Melastatin 2 (TRPM2) ion channel is required for innate immunity against Listeria monocytogenes. Proc Natl Acad Sci U S A. 2011; 108:11578–11583. [PubMed: 21709234]

17. Algood HM, Cover TL. Helicobacter pylori persistence: an overview of interactions between H. pylori and host immune defenses. Clin Microbiol Rev. 2006; 19:597–613. [PubMed: 17041136]
18. Naito Y, Yoshikawa T. Molecular and cellular mechanisms involved in Helicobacter pylori-induced inflammation and oxidative stress. Free Radic Biol Med. 2002; 33:323–336. [PubMed: 12126754]
19. Mantovani A, Sozzani S, Locati M, Allavena P, Sica A. Macrophage polarization: tumor-associated macrophages as a paradigm for polarized M2 mononuclear phagocytes. Trends Immunol. 2002; 23:549–555. [PubMed: 12401408]
20. Martinez FO, et al. Genetic programs expressed in resting and IL-4 alternatively activated mouse and human macrophages: similarities and differences. Blood. 2013; 121:e57–69. [PubMed: 23293084]
21. Harris PR, et al. Recombinant Helicobacter pylori urease activates primary mucosal macrophages. J Infect Dis. 1998; 178:1516–1520. [PubMed: 9780278]
22. Gobert AP, et al. Helicobacter pylori heat shock protein 60 mediates interleukin-6 production by macrophages via a toll-like receptor (TLR)-2-, TLR-4-, and myeloid differentiation factor 88-independent mechanism. J Biol Chem. 2004; 279:245–250. [PubMed: 14573621]
23. Wilson KT, Crabtree JE. Immunology of *Helicobacter pylori*: insights into the failure of the immune response and perspectives on vaccine studies. Gastroenterology. 2007; 133:288–308. [PubMed: 17631150]
24. Mizuno T, et al. Interleukin-17 levels in *Helicobacter pylori*-infected gastric mucosa and pathologic sequelae of colonization. World J Gastroenterol. 2005; 11:6305–6311. [PubMed: 16419159]
25. Handa O, Naito Y, Yoshikawa T. Redox biology and gastric carcinogenesis: the role of Helicobacter pylori. Redox Rep. 2011; 16:1–7. [PubMed: 21605492]
26. Cross AR, Jones OT. The effect of the inhibitor diphenylene iodonium on the superoxide-generating system of neutrophils. Specific labelling of a component polypeptide of the oxidase. Biochem J. 1986; 237:111–116. [PubMed: 3800872]
27. Bulua AC, et al. Mitochondrial reactive oxygen species promote production of proinflammatory cytokines and are elevated in TNFR1-associated periodic syndrome (TRAPS). J Exp Med. 2011; 208:519–533. [PubMed: 21282379]
28. Naik E, Dixit VM. Mitochondrial reactive oxygen species drive proinflammatory cytokine production. J Exp Med. 2011; 208:417–420. [PubMed: 21357740]
29. Bedard K, Krause KH. The NOX family of ROS-generating NADPH oxidases: physiology and pathophysiology. Physiol Rev. 2007; 87:245–313. [PubMed: 17237347]
30. Griendling KK, Sorescu D, Lassegue B, Ushio-Fukai M. Modulation of protein kinase activity and gene expression by reactive oxygen species and their role in vascular physiology and pathophysiology. Arterioscler Thromb Vasc Biol. 2000; 20:2175–2183. [PubMed: 11031201]
31. Bhattacharyya A, et al. Mitogen-activated protein kinases and nuclear factor-kappaB regulate Helicobacter pylori-mediated interleukin-8 release from macrophages. Biochem J. 2002; 368:121–129. [PubMed: 12150710]
32. Pathak SK, et al. TLR4-dependent NF-kappaB activation and mitogen- and stress-activated protein kinase 1-triggered phosphorylation events are central to Helicobacter pylori peptidyl prolyl cis-, trans-isomerase (HP0175)-mediated induction of IL-6 release from macrophages. J Immunol. 2006; 177:7950–7958. [PubMed: 17114467]
33. Zhao Y, et al. Helicobacter pylori heat-shock protein 60 induces interleukin-8 via a Toll-like receptor (TLR)2 and mitogen-activated protein (MAP) kinase pathway in human monocytes. J Med Microbiol. 2007; 56:154–164. [PubMed: 17244794]
34. Nunez-Villena F, et al. Increased expression of the transient receptor potential melastatin 7 channel is critically involved in lipopolysaccharide-induced reactive oxygen species-mediated neuronal death. Antioxid Redox Signal. 2011; 15:2425–2438. [PubMed: 21539414]
35. Su LT, et al. TRPM7 activates m-calpain by stress-dependent stimulation of p38 MAPK and c-Jun N-terminal kinase. J Mol Biol. 2010; 396:858–869. [PubMed: 20070945]
36. Inoue H, Murayama T, Tashiro M, Sakurai T, Konishi M. Mg(2+)- and ATP-dependent inhibition of transient receptor potential melastatin 7 by oxidative stress. Free Radic Biol Med. 2014; 72:257–266. [PubMed: 24747489]

37. Hoth M, Penner R. Depletion of intracellular calcium stores activates a calcium current in mast cells. Nature. 1992; 355:353–356. [PubMed: 1309940]
38. Feske S, et al. A mutation in Orai1 causes immune deficiency by abrogating CRAC channel function. Nature. 2006; 441:179–185. [PubMed: 16582901]
39. Vig M, et al. CRACM1 is a plasma membrane protein essential for store-operated Ca2+ entry. Science. 2006; 312:1220–1223. [PubMed: 16645049]
40. Montell C. The TRP superfamily of cation channels. Sci STKE. 2005; 2005:re3. [PubMed: 15728426]
41. Hogan PG, Rao A. Dissecting ICRAC, a store-operated calcium current. Trends Biochem Sci. 2007; 32:235–245. [PubMed: 17434311]
42. Robinson LC, Marchant JS. Calcium influx: beyond ‘current’ biology. Curr Biol. 2006; 16:R548–550. [PubMed: 16860734]
43. Partida-Sanchez S, et al. Chemotaxis of mouse bone marrow neutrophils and dendritic cells is controlled by adp-ribose, the major product generated by the CD38 enzyme reaction. J Immunol. 2007; 179:7827–7839. [PubMed: 18025229]
44. Knowles H, et al. Transient Receptor Potential Melastatin 2 (TRPM2) ion channel is required for innate immunity against Listeria monocytogenes. P Natl Acad Sci USA. 2011; 108:11578–11583.
45. Qian X, et al. Transient receptor potential melastatin 2 protects mice against polymicrobial sepsis by enhancing bacterial clearance. Anesthesiology. 2014; 121:336–351. [PubMed: 24781495]
46. Wehrhahn J, Kraft R, Harteneck C, Hauschildt S. Transient receptor potential melastatin 2 is required for lipopolysaccharide-induced cytokine production in human monocytes. J Immunol. 2010; 184:2386–2393. [PubMed: 20107186]
47. Kim HR, et al. Reactive oxygen species prevent imiquimod-induced psoriatic dermatitis through enhancing regulatory T cell function. PLoS One. 2014; 9:e91146. [PubMed: 24608112]
48. Efimova O, Szankasi P, Kelley TW. Ncf1 (p47phox) is essential for direct regulatory T cell mediated suppression of CD4+ effector T cells. PLoS One. 2011; 6:e16013. [PubMed: 21253614]
49. Brechard S, Tschirhart EJ. Regulation of superoxide production in neutrophils: role of calcium influx. J Leukoc Biol. 2008; 84:1223–1237. [PubMed: 18519744]
50. Barbet G, et al. The calcium-activated nonselective cation channel TRPM4 is essential for the migration but not the maturation of dendritic cells. Nat Immunol. 2008; 9:1148–1156. [PubMed: 18758465]
51. Foyouzi-Youssefi R, Petersson F, Lew DP, Krause KH, Nusse O. Chemoattractant-induced respiratory burst: increases in cytosolic Ca2+ concentrations are essential and synergize with a kinetically distinct second signal. Biochem J. 1997; 322(Pt 3):709–718. [PubMed: 9148740]
52. Granfeldt D, Samuelsson M, Karlsson A. Capacitative Ca2+ influx and activation of the neutrophil respiratory burst. Different regulation of plasma membrane- and granule-localized NADPH-oxidase. J Leukoc Biol. 2002; 71:611–617. [PubMed: 11927647]
53. Gallois A, Bueb JL, Tschirhart E. Effect of SK&F 96365 on extracellular Ca2+-dependent O2- production in neutrophil-like HL-60 cells. Eur J Pharmacol. 1998; 361:293–298. [PubMed: 9865520]
54. Aarts M, et al. A key role for TRPM7 channels in anoxic neuronal death. Cell. 2003; 115:863–877. [PubMed: 14697204]
55. Chen HC, Su LT, Gonzalez-Pagan O, Overton JD, Runnels LW. A key role for Mg(2+) in TRPM7’s control of ROS levels during cell stress. Biochem J. 2012; 445:441–448. [PubMed: 22587440]
56. Chaturvedi R, et al. L-arginine availability regulates inducible nitric oxide synthase-dependent host defense against Helicobacter pylori. Infect Immun. 2007; 75:4305–4315. [PubMed: 17562760]
57. Gu Y, Barry J, Gu C. Kv3 channel assembly, trafficking and activity are regulated by zinc through different binding sites. Journal of Physiology. 591:2491–2507.

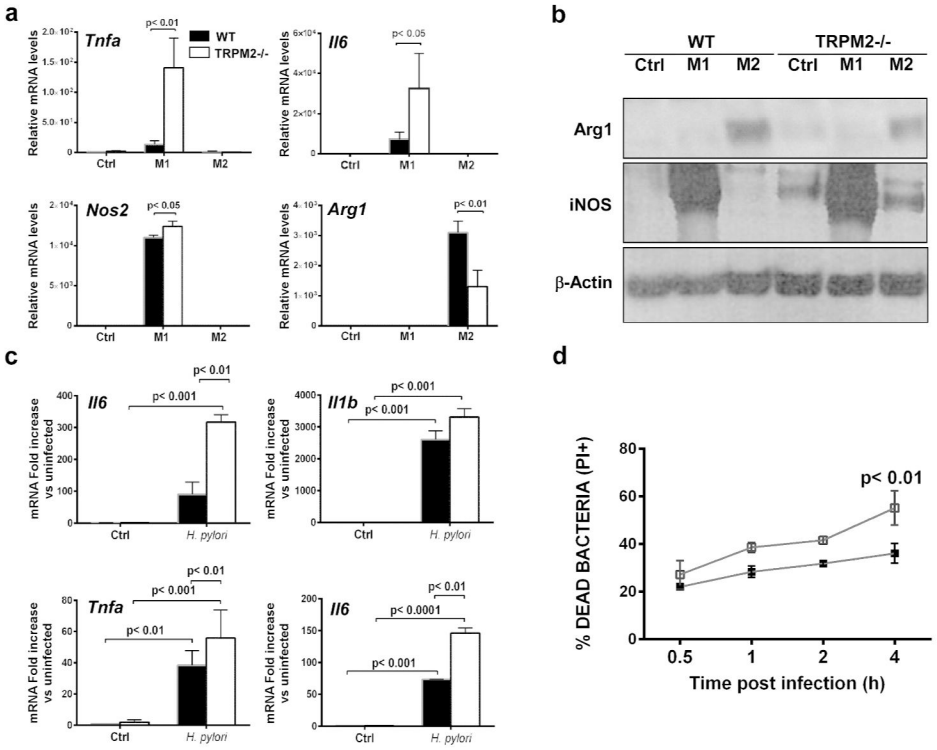

Figure 1. TRPM2 deficiency results in increased classical M1 polarization in vitro and in vivo

(a) Expression of genes associated with macrophage polarization in BMDM after 6 h of stimulation with M1-polarizing stimuli, LPS (50 ng/ml) and IFN-γ (20 ng/ml), or M2-polarizing stimuli, IL-4 (20 ng/ml) and IL-13 (20 ng/ml). *Tnfa, il6, Nos2 and Arg1* expression levels were assessed by qRT-PCR and normalized to *Gapdh* levels. Data shown are representative of four independent experiments. (b) Arg1 and iNOS protein levels were assessed by Western blotting after 24 h of M1-and M2-polarizing stimuli treatment of BMDM cells from WT and *Trpm2*$^{-/-}$ mice. A representative blot is shown. Similar results were observed in three independent experiments. (c) BMDM from WT and *Trpm2*$^{-/-}$ mice were stimulated with *H. pylori* for 6 h, and RNA was isolated and subjected to qRT-PCR analysis of *Il12p40*, *Il1b*, *Tnfa* and *Il6*. Expression was normalized to GAPDH. The values shown are from four independent experiments. (d) Flow cytometry analysis of bactericidal activity. BMDM from WT and *Trpm2*$^{-/-}$ mice were incubated with *H. pylori* (MOI of 10) for 1 h. Cells were then washed and further incubated for 0–4 h, then lysed. The lysates were exposed to Syto 9 and propidium iodide (PI) to stain live and dead bacteria, respectively. Percentage of PI^{+} cells from 0.5 to 4 h after challenge is shown. (c–d) Data are representative of five independent experiments.

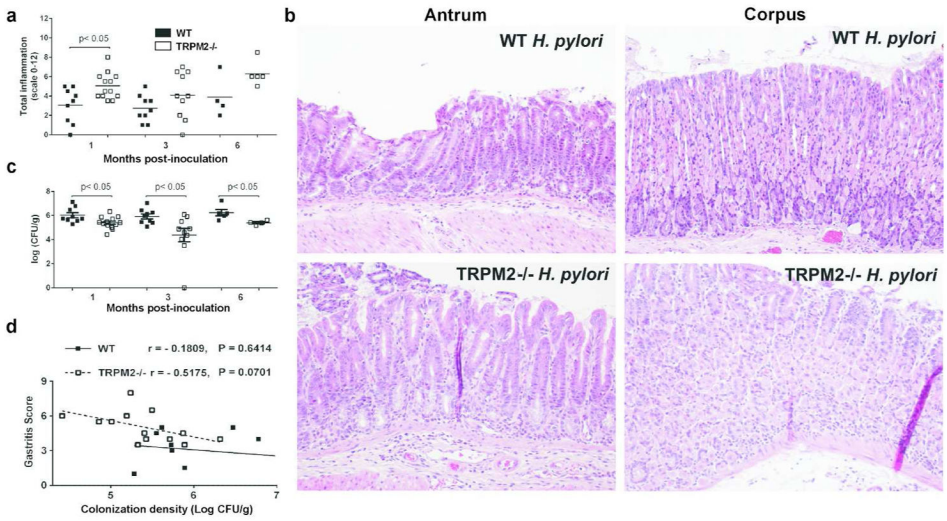

Figure 2. Lack of TRPM2 improves control of *Helicobacter pylori* infection but aggravates gastric immunopathology

(a) Gastric inflammation at 1, 3 and 6-mo after *H. pylori* PMSS1 infection was assessed and scored (0 to 12) on stomach tissue (corpus and antrum) in WT and T *Trpm2*$^{-/-}$ mice. Each data point represents inflammation scores from an individual animal. (b) Representative histologic images from *H. pylori*-infected WT antrum, *H. pylori*-infected WT corpus, *H. pylori*-infected TRPM2$^{-/-}$ antrum, *H. pylori*-infected TRPM2$^{-/-}$ corpus mice at 200x magnification. (c) Levels of colonization were measured by plating serial dilutions of stomach homogenates. The number of CFU was then calibrated to the weight of the tissue and log CFU/g is presented on the graphs. (d) Colonization was plotted against total inflammation for each infected mouse. The lines illustrate the best-fit linear regressions obtained for the two strains of mice with the correlation coefficient and significance as indicated. Each point represents a single mouse. Similar results were also observed in two other independent experiments. Results from experiments with 4–13 mice per group and are representative of at least three independent experiments.

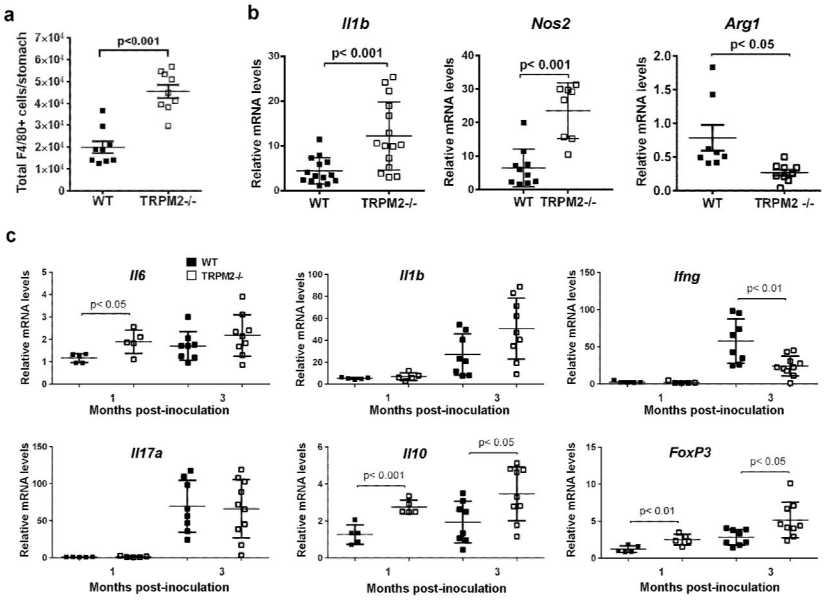

Figure 3. Innate, but not adaptive, inflammatory responses are increased in *H. pylori*-infected *Trpm2*$^{-/-}$ mice

Gastric cells were isolated from *H. pylori* infected WT and Trpm2−/− mice sacrificed at 1-mo after challenge, and analyzed by flow cytometry for the expression of the macrophage marker F4/80. Total number of of F4/80+ (gated on CD11b+ and Ly6C+) cells per stomach is shown. (a) F4/80+ cells were isolated from the stomachs of WT and Trpm2−/− mice challenged with *H. pylori*, by magnet-assisted cell sorting (MACS). (b) RNA was isolated from macrophages and qRT-PCR was performed to analyze expression of *Il1b, Nos2* and *Arg1*. Expression was normalized to *Gapdh*. Each point represents data from an individual animal. Results shown are from experiments with 8 to 15 mice per group. Similar results were observed in two other independent experiments. WT and *Trpm2*$^{-/-}$ mice were infected with *H. pylori*. At 1 and 3-mo post-infection, mice were sacrificed, gastric tissues were removed, and RNA was extracted. (c) Relative mRNA levels of *Il6, Il1b, and Ifng* (top panel) or *Il17a, Il10,* and *Foxp3* (bottom panel) were measured by qRT-PCR. All qRT-PCR data were standardized to *Gapdh* mRNA. Relative mRNA levels of each point represent a single mouse. Results from experiments with 4 to 13 mice per group and are representative of at least three independent experiments.

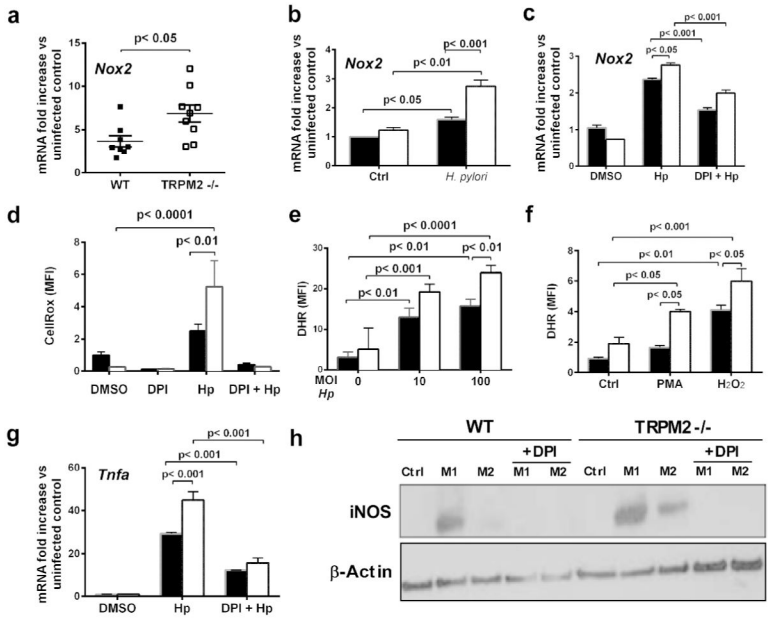

Figure 4. TRPM2 deficiency promotes NAPDH oxidase activity and oxidative stress during infection with *H. pylori*

(a) *Nox2* mRNA levels were measured by qRT-PCR from the stomach of *H. pylori*-infected WT and *Trpm2*$^{-/-}$ mice sacrificed at 3-mo after challenge. Data were standardized to *Gapdh*. Each point represents a single mouse. (b) *Nox2* transcript abundance in WT and TRPM2$^{-/-}$ BMDM was determined by qRT-PCR, and values were normalized with respect to *Gapdh* mRNA. (c) qRT-PCR analysis of *Nox2* mRNA levels from WT and TRPM2 BMDM stimulated with *H. pylori*, and pretreated with DPI when indicated. Values were normalized with respect to *Gapdh* mRNA. (d) Release of ROS, assessed as CellROX fluorescence in WT and TRPM2$^{-/-}$ BMDM left unstimulated (DMSO) or stimulated with *H. pylori* (MOI of 50), or additional pretreatment with DPI (10 μM), presented as relative fluorescence. (e) H_2O_2 release measured by DHR123 oxidation in controls and *H. pylori*-stimulated WT and TRPM2$^{-/-}$ BMDM, presented as relative fluorescence. (f) Assessment of H_2O_2 release by DHR123 fluorescence in WT and TRPM2$^{-/-}$ BMDM left unstimulated (Control), or stimulated with PMA (1 μM) or H_2O_2 (10 μM), presented as relative fluorescence. (g) WT and TRPM2$^{-/-}$ BMDM were infected with *H. pylori*, with or without pretreatment with DPI (10 μM), and expression of *Tnfa* was examined by qRT-PCR analysis. (b–g) The values shown are from four independent experiments. (h) WT and TRPM2$^{-/-}$ BMDM were infected with *H. pylori*, with or without pretreatment with DPI (10 μM), and protein level of iNOS was examined by Western blot analysis. Data were standardized to β-actin. Western blots are representative of three independent experiments with similar results.

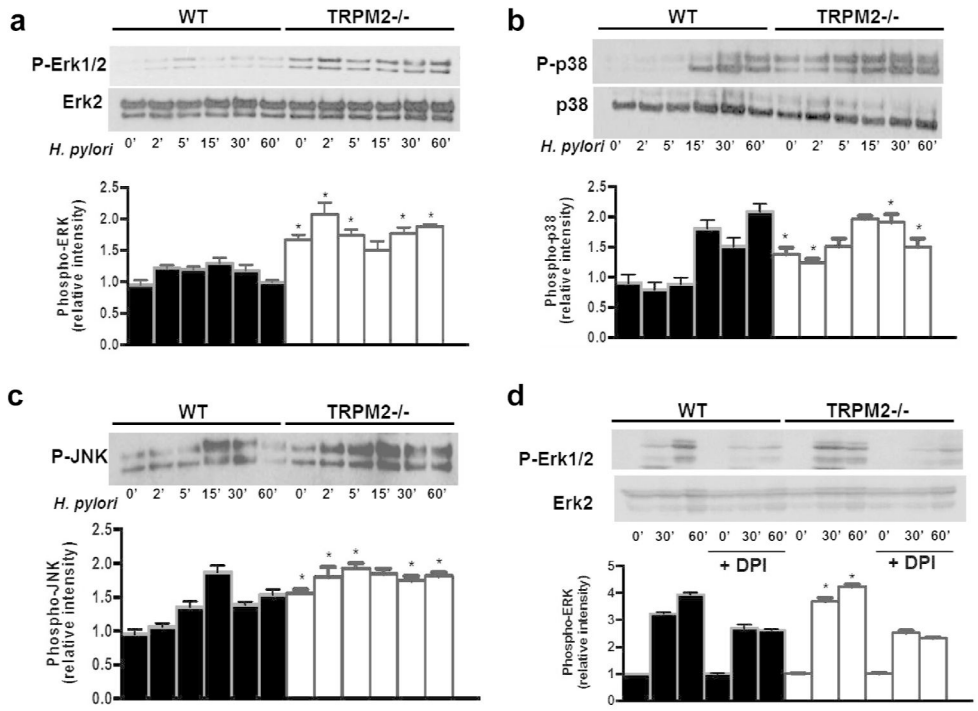

Figure 5. TRPM2 ablation augments *H. pylori*-induced MAPK activation

BMDM from WT and *Trpm2*$^{-/-}$ mice were co-cultured with *H. pylori* (MOI of 10) for the indicated time points, and activity of ERK (a), p38 (b) and JNK (c) were examined by Western blot analysis using phosphospecific antibodies. The total protein levels of ERK and p38 were also measured. (d) WT and TRPM2$^{-/-}$ BMDM were pretreated with DMSO or DPI (10 μM) before stimulation with *H. pylori* at the indicated times. The phosphorylation of ERK1/2 was analyzed by Western blot. (ad) Densitometric analysis for each MAPK band is displayed beneath Western blot respectively. Western blots shown are representative of three independent experiments with similar results. Statistical analyses are performed comparing differences between WT and TRPM2−/− cells at each time point (*p<0.05).

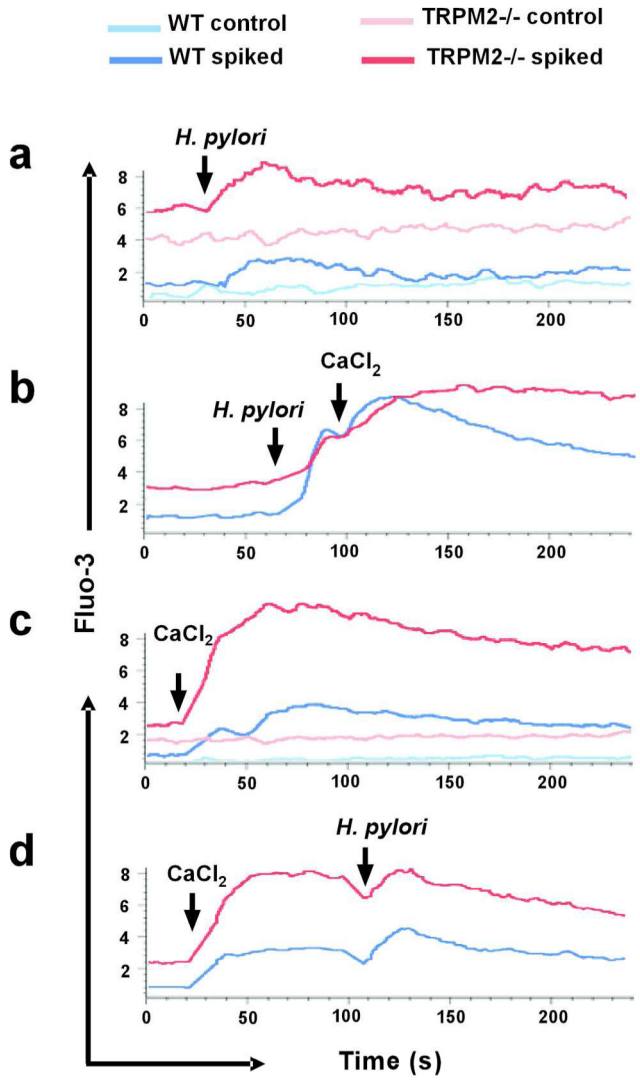

Figure 6. *H. pylori* modulates intracellular Ca^{2+} levels in macrophages

Free intracellular Ca^{2+} levels were measured by flow cytometry in WT and TRPM2$^{-/-}$ BMDM loaded with the fluorescent Ca^{2+} indicator Fluo-3. Cells were spiked with (a) *H. pylori* (MOI of 100), (b) *H. pylori* followed by $CaCl_2$ (2 mM), (c) $CaCl_2$ (2 mM), or (d) $CaCl_2$ (2 mM) followed by *H. pylori* at the indicated time. Accumulation of free Ca^{2+} was measured by flow cytometry over the next 4 min. One of three independent experiments is shown.

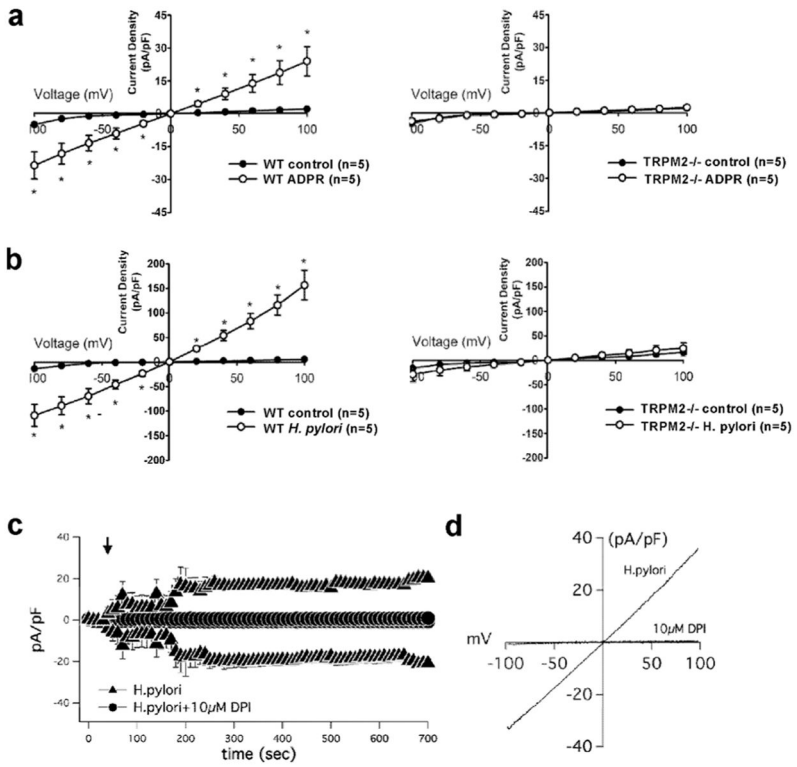

Figure 7. *H. pylori* modulates membrane conductance of macrophages through TRPM2

(a) I-V relationship of *H. pylori*-induced membrane conductance in WT and TRPM2$^{-/-}$ cells. Current traces of WT (left panel) or TRPM2$^{-/-}$ (right panel) BMDM by voltage-clamp recording when perfused with control, (a) ADPR (200 μM) or (b) *H. pylori* suspension at 1×10^6 CFU/mL. (c) BMDM were suspended in Hank's buffer with (circles) or without (triangles) DPI (10 μM), then electrophysiological measurements were recorded in whole-cell configuration for temporal development of inward and outward currents in WT cells by voltage-clamp recordings when cells were perfused with *H. pylori* containing buffer. (d) Current/voltage (IV) relationship of *H. pylori* alone (*H. pylori*), and *H. pylori* in WT cells preincubated with 10 μM DPI. Data are expressed as mean ± SEM, n=7–20.

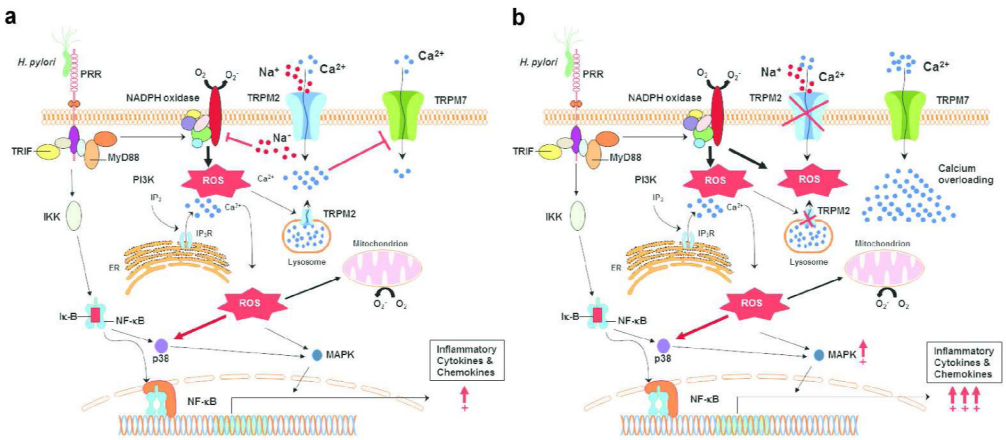

Figure 8. Model of TRPM2 mediated signaling mechanisms in macrophages during *H. pylori* infection

(a) *H. pylori* engages pattern of recognition receptors (PRRs), *e.g.* toll-like receptors (TLRs), which recruit MyD88 and TRIF adaptor proteins that may trigger the activation of phosphatidylinositol 3-kinase (PI3K), followed by an increase of intracellular concentration of Ca^{2+} via release of inositol-1,4,5-trisphosphate Ins(1,4,5)P_3R channel located on the endoplasmic reticulum (ER) or putative expression of lysosomal TRPM2 channel, respectively. The rise in the cytosolic Ca^{2+} concentration and the activity of PI3K lead to the activation of mitogen activated kinases (MAPK) and other kinases that phosphorylate the cytosolic subunits of the NADPH oxidase of phagocytes, activating their migration to the plasma membrane and enhancing production of reactive oxygen species (ROS). Increased ROS contributes to increased inflammatory gene expression through Ca^{2+}-dependent signaling pathways, such as MAPK and NF-κB transcription factors. Oxidants, including H_2O_2, may mobilize ADPR from mitochondria (both H_2O_2 and Ca^{2+} can synergize with ADPR to activate TRPM2) stimulating additional cation entry across plasma membrane TRPM2. Intracellular accumulation of Na^+ through TRPM2 mediates membrane depolarization, which inhibits NADPH oxidase activity, then limiting the inflammatory cascade. (b) In the absence of TRPM2, the initial PI3K dependent, IP_3 mediated spike of cytosolic Ca^{2+} will rapidly return to baseline levels. Moreover, NADPH oxidase activity will not be restricted, resulting in further increment in ROS accumulation, and consequently, dysregulated enhancement of inflammatory signaling pathways. Persistent cell stimulation by *H. pylori* in the TRPM2 knockout will result in transitory Ca^{2+} starvation that may be the driving force for the opening of additional cation channels at the plasma membrane (e.g. TRPM7), which will enable compensatory mechanisms of Ca^{2+} entry favoring cytosolic Ca^{2+} overload, and hence, the extension of exacerbated inflammatory signals.